Large-scale testing of a hydraulic non-linear mooring system for floating offshore wind turbines

Magnus J. Harrold[a], Philipp R. Thies[a,*], David Newsam[b], Claudio Bittencourt Ferreira[c], Lars Johanning[a]

[a] *The University of Exeter, College of Engineering, Mathematics and Physical Sciences, Penryn, Cornwall, UK;*
[b] *Teqniqa Systems Ltd., London, UK;*
[c] *DNV GL, London, UK;*

Abstract

The mooring system has been recognised as a key area of expense that needs to be addressed to improve the cost competitiveness of floating offshore wind turbines. The devices installed to date have generally adopted designs from the oil and gas industry using heavy mooring materials, providing the required safety margins but with a significant degree of conservatism. Recent interest in the usage of lighter and more compliant mooring materials has shown that they have the potential to reduce peak line loads, which would in-turn reduce costs. However, the lack of operational experience with such materials has limited their adoption in a risk averse industry. This paper reports on the large-scale physical testing of a hydraulic-based mooring component with non-linear stiffness characteristics. The performance of the device is characterised in a laboratory both statically and dynamically, as well as in conditions representative of operating in a sea state using a combined physical and numerical modelling approach. The results show that the dynamic stiffness of the component is a function of load history and hydraulic pre-charge pressure, while the inclusion of the device as part of the OC4 semi-submersible floating wind platform can reduce the peak mooring line loads by up to 9%. Beyond the physical test results, the calculations suggest that the peak load reduction in the modelled scenarios could

*Corresponding author
Email address: p.r.thies@exeter.ac.uk (Philipp R. Thies)

be as much as 40% if the device can be scaled further. The paper supports the adoption of innovative mooring systems through dedicated component and performance testing.

Keywords: floating wind energy, mooring systems, physical testing, numerical modelling

---

1. Introduction

The offshore wind energy industry has continued to make significant progress in recent years, with Europe adding 2.6 GW of installed capacity in 2018 alone, or just over 400 turbines [1]. These installations have almost entirely used bottom-fixed foundations, with monopiles and to a lesser extent jacket structures being the foundation of choice [2]. While the progress to date has been impressive, bottom-fixed technology is currently limited to shallow water depths (<50 m) due to a number of challenges associated with sizing and installing these sub-structures in deeper waters. However, the majority of the offshore wind energy resource is found in deep water. For example, 66% of the North Sea has a water depth between 50 - 220 m, and it has been estimated that this area alone could meet the EU's electricity consumption 4 times over [3]. This has led to increased interest in alternative solutions to access this resource. Floating offshore wind turbines (FOWT) are increasingly showing promise for tackling deeper water sites, with several, global installations of FOWT on an individual basis in recent years [4, 5], while the Worlds first pilot farm became operational in 2017 [6].

These initial FOWT projects have primarily used semi-submersible or spar buoy based foundations, with conventional, catenary mooring systems based on designs from the oil and gas industry. However, at present there is a degree of conservatism and over-engineering in these mooring systems due to a lack of relevant standards [7], resulting in expensive designs and a preference for heavy steel and wire materials. It has been highlighted that the mooring system can account for in excess of 10% of the overall FOWT CapEx [8], implying that this is a key area where the overall cost-competitiveness with more established forms of energy generation could be improved.

The usage of synthetic mooring materials for FOWT could deliver considerable cost reductions, since these are both cheaper and lighter than heavy moorings with equivalent breaking strengths [9]. The weight savings from using synthetic rope would also lower the vessel requirements during installation, bringing further cost reduction [7]. Synthetic materials lie within the category of non-linear mooring systems, whereby the line is initially soft and elastic, before the stiffness increases significantly at higher extensions. If used alongside other, conventional materials as part of a hybrid mooring system, this non-linear response reduces the tensions developed in mooring lines without sacrificing the overall platform survivability, meaning that lower strength, and hence cost, moorings could be used instead.

A number of novel mooring systems with heightened non-linear characteristics have been proposed for offshore renewable energy applications in recent years, including those comprised of elastomeric [10] and combined elastomeric-thermoplastic materials [11]. These mooring systems can introduce significantly lower axial stiffness than synthetic ropes, reducing line tensions further and potentially offering even greater cost reductions [12]. However, the challenge for all non-linear mooring materials is that they exhibit stiffness characteristics that are dependent on load history [13], which need to be quantified to support their application in the conservative FOWT industry. In addition to this, a better understanding of fatigue life is required to prove the suitability of such materials over the 25 - 30 year lifetime of a FOWT [7].

This paper reports on the large-scale performance testing of a hydraulic mooring component with non-linear stiffness characteristics due to the developed tensile forces compressing a pressurised bladder, storing energy in a manner analogous to a piston rod retracting into a hydraulic cylinder [14]. The component is referred to as the Intelligent Mooring System (IMS) since the pre-charge pressure can be varied, which in turn allows a multitude of stiffness responses. This is the key advantage that the IMS offers over the other aforementioned non-linear mooring systems. The paper is structured as follows: Section 2 details the test setup, including the IMS prototype, the component test rig and the required pre-conditioning of the device; Section 3 states the various methods used to characterise the static and dynamic performance of the IMS, as well as the testing of the device in a simulated offshore environment using a combined numerical and physical modelling approach; Section 4 reports on the results from each of the performance tests; Section 5 discusses the importance and load reduction benefits for the FOWT application; while Section 6 concludes with the implications for technology development and mooring design.

2. Test Setup

2.1. IMS Prototype

The IMS comprises two key parts: a hollow braided Vectran rope that houses a pressurised water filled bladder; and a gas-charged accumulator. As the rope extends under tension, the volume of the internal bladder compresses and water is transferred to the accumulator. This acts as a means of storing the energy from the loading event, reducing the tension developed in the line and providing an overall functionality akin to a shock absorber. These load reduction properties could be exploited by placing IMS units at the end of each mooring line of a FOWT, alongside the existing conventional line material used elsewhere. It is anticipated that the devices would be placed at the platform end of each line to improve access for inspection and maintenance, while as many as 3 units would be placed in parallel on each line to provide redundancy.

The IMS was built at prototype scale (Figure 1) by Teqniqa Systems Ltd. in order to advance the device to a technology readiness level (TRL) of 5 - 6. This follows on from previous work in which the device progressed to a TRL level of 4 through proof-of-concept testing [15, 16]. The IMS has been advanced in this work by integrating the braided rope and accumulator into a single unit in a configuration that is representative of how the anticipated commercial design will be in-line and part of the rest of the mooring system. Previously the device

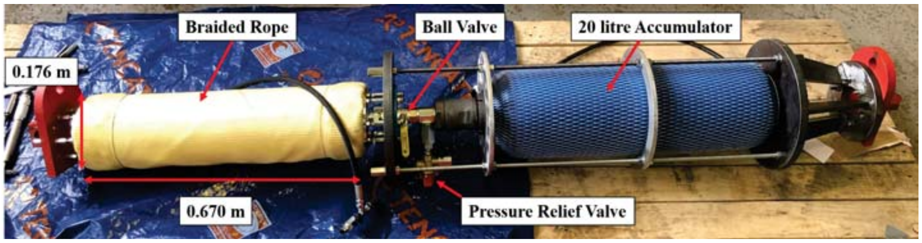

Figure 1: Intelligent Mooring System (IMS)

Figure 2: DMaC test rig with IMS installed (left); close-up of the IMS submerged in DMaC (right)

featured an accumulator that was external to the braid and was connected to the bladder via extensive pipework in order to demonstrate the working principles. The braided rope in the new device has a length of 670 mm and a diameter of 176 mm, while the accumulator has a volume of 20 litres. A ball valve and pressure relief valve were placed between the accumulator and bladder.

2.2. Test Rig and Instrumentation

The IMS was tested at the University of Exeter's Dynamic Marine Component Test Facility, or DMaC for short. DMaC is a tensile test machine that can replicate the motions and forces that mooring lines and subsea cables are subject to [17]. This is achieved via a linear hydraulic cylinder that applies tensile forces to test samples, either through operation in displacement or force mode.

The tensile loading on the IMS was measured by a DSCC pancake load cell, manufactured by Applied Measurements. This sensor was placed on the DMaC piston and has a full-scale linearity of 0.039%. A WS12 draw-wire transducer, also manufactured by Applied Measurements, was used to measure the IMS elongation. The validity of the data from this sensor was verified against the independent DMaC piston displacement measurements, which were obtained at a resolution of 0.05 mm using a LM10 linear encoder manufactured by RLS. Piezo-resistive pressure sensors with an accuracy of 0.25% were placed on both the IMS accumulator and bladder. The measurements from all of the aforementioned sensors were recorded using a National Instruments (NI) CompactRIO 9022 at a sampling rate of 50 Hz and synchronized to a common timestamp. Load measurements utilised a NI 9237 C-Series module and displacement measurements used a NI 9205 C-Series module for the CompactRIO.

2.3. Sample Preparation

The IMS accumulator pre-charge pressure has a direct influence on its performance characteristics, as detailed in [15]. For this test campaign, three precharge configurations were chosen to further study these effects, specifically 162, 252 and 310 kPa. The accumulator pre-charge was manually set to these values via a manual pump whilst isolated from the bladder. The two sub-systems were then re-connected and an external water source was used to pressurise the bladder to the same level. The readings from the pressure sensors were monitored throughout this process to ensure that no water inadvertently entered the accumulator. Thus the total fluid in the system for each configuration is the same and equivalent to the bladder volume at 0% extension. Whilst it was shown in previous work that varying the total fluid in the system also has an influence on the performance characteristics [15], this was deemed to be insignificant in this study due to the small volume of the accumulator relative to the bladder.

DMaC was flooded with freshwater for the duration of the test campaign, ensuring that the IMS was tested in a submerged condition representative of its intended application. The IMS was then subject to a standard bedding-in procedure to condition the rope to a known, repeatable state, as described in Section B3.1 in ISO/TS 19336:2015 [18]. The procedure is briefly described as follows:

- Apply a load of 2% of the minimum breaking strength (MBS)
- Pull to a load of 50% of the MBS at a rate of 10% MBS per minute and hold for 30 minutes
- Reduce the load to 10% MBS at a rate of 10% MBS per minute
- Cycle between 10% and 30% MBS at a frequency of 0.05 Hz for 100 cycles
- Unload

The MBS was not known at the time of testing and instead this figure was based on the lowest load that led to an ultimate strength failure during prior work in commissioning the device. Figure 3 shows the IMS bedding-in procedure in terms of both tension and extension. During the static hold at 50% MBS, two audible sounds were heard from the braid at approximately 500 and 1620 seconds, the second of which is highlighted in Figure 3. Both of these events caused a small spike in the controlled tension and a minor step change in the braid extension. The events are believed to be a result of the macroscopic alignment of braid fibres under this initial loading period. Overall only a small amount of creep is observed during the entire 30 minute static hold, with the extension increasing from 49.3% to 49.7%, or less than 3 mm. During the subsequent cycling of the device, it is observed that the extension amplitude decreases slightly before it can be considered that the performance of the IMS reaches a repeatable state.

3. Performance Test Methodology

3.1. Static Characterisation

The first IMS performance test aimed to characterise the semi-static load-extension behaviour of the device. This was achieved by slowly pulling the braid

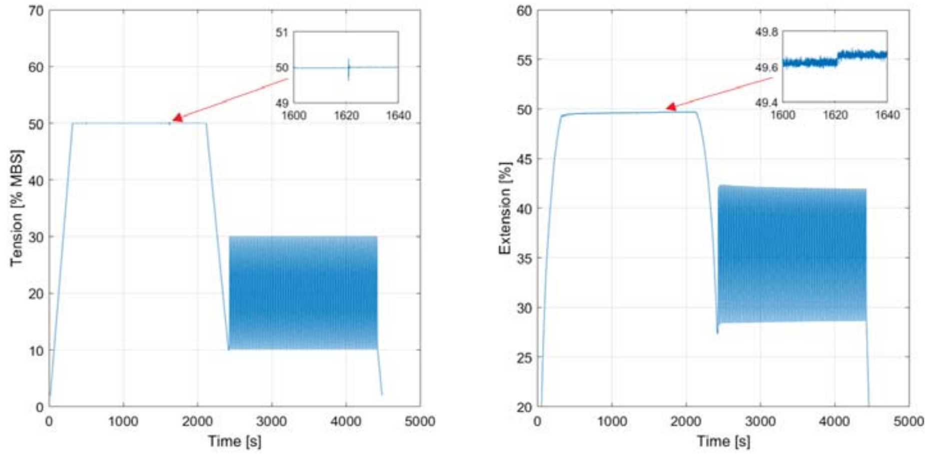

Figure 3: Bedding-in procedure for the IMS in terms of tension (left) extension (right). The insets highlight a period in which a minor braid alignment occurred

in a defined series of displacement steps, whereby the test rig was commanded to hold the braid extension constant for a period of 30 seconds until moving to the next step. A linear ramp with a period of 30 seconds was used between steps. This process was followed until reaching approximately 50% braid extension, after which the same stepping points were also captured during retraction using this method. The semi-static test profile is shown in Figure 4.

3.2. Dynamic Characterisation

The performance of the device was further characterised under dynamic conditions, where the braid was cycled within the extension range 15 - 45% at a number of frequencies, from less than 0.01 Hz to 0.1 Hz. The device was cycled 20 times during each test, consistent with the dynamic performance characterisation of a previous prototype [16]. The dynamic test profile for the 0.033 Hz cycling frequency is shown in Figure 5.

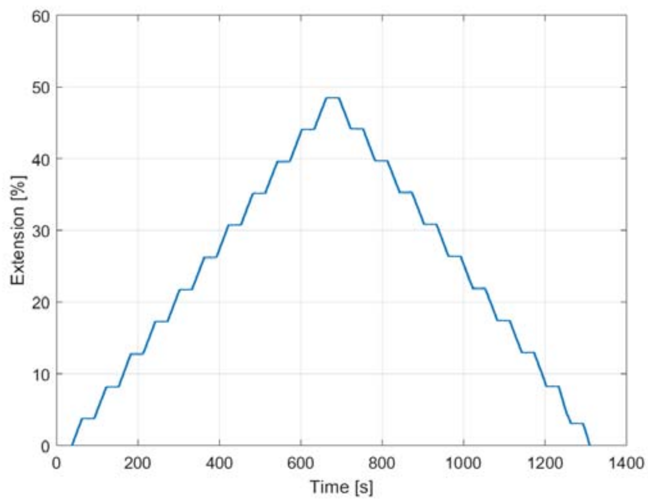

Figure 4: Semi-Static performance test profile

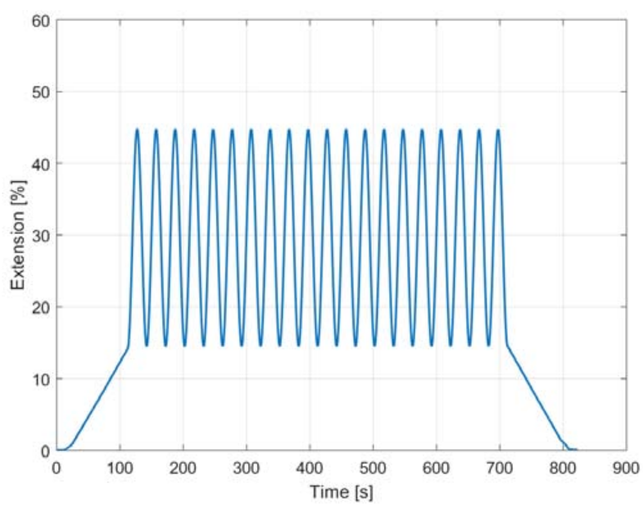

Figure 5: 0.033 Hz Dynamic performance test profile

3.3. Representative Testing

3.3.1. Numerical Model

After characterising the performance of the IMS in both static and dynamic conditions, the final objective of the test campaign involved subjecting the device to conditions representative of an offshore deployment. In the absence of field measurements, the conditions were instead derived from a FAST-OrcaFlex [19] numerical model of a FOWT. FAST [20] is a validated engineering tool for simulating the response of onshore and offshore wind turbines, coupling models of aerodynamics, hydrodynamics, servo-dynamics and structural dynamics. Meanwhile OrcaFlex [21] is a finite element model developed by Orcina for the dynamic analysis of offshore systems, including floating platforms, vessels, pipelines and mooring systems. In the combined FAST-OrcaFlex model, FAST essentially accounts for the structure and dynamics above the water surface as well as the platform global motion, while OrcaFlex models the mooring lines and hydrodynamics below the water surface.

The platform considered is the OC4 semi-submersible [22], which features the baseline NREL 5 MW wind turbine and a conventional 3-line catenary mooring system. This was modified in OrcaFlex to include the IMS as part of the FOWT by removing a small length of the default mooring system with an equivalent length of a new line segment that features the mean non-linear load-extension curves measured from the semi-static performance characterisation tests (Section 4.1). Three of these new segments were placed in parallel on each mooring line to provide further stiffness, akin to the envisaged IMS final design. The loading requirements of the IMS were derived in previous work [23] from simulations of the default FOWT arrangement, i.e. without the inclusion of the IMS. The measured performance characteristics of the IMS prototype, shown later in Section 4, were Froude scaled up by a factor of 4 to meet these loading requirements. Therefore, in the numerical model each IMS unit has a braid length of 2.67 m.

Table 1 summarises the properties of the mooring system in the numerical model, with each line comprising of segments of the default mooring and the IMS. Note that the IMS properties vary as a function of extension, as denoted by the range of values provided for the length and axial stiffness. However, it was not possible to model the diameter and mass density in this way, with the values stated instead representing typical operational figures. The IMS axial stiffness stated is for a single unit, meaning that by placing three units in parallel on each line the overall stiffness triples. The default mooring properties are as described in [22], with the only change being a slight reduction in the segment length to accommodate the IMS, as stated previously. No information is provided on where the default mooring properties are derived from, although one of the authors in a similar, previous project [24] simplified the mooring system for the OC3 spar buoy by modelling a homogeneous line with the weighted average properties of the actual multi-segment line used in the concept design. It is assumed that a similar approach was used for the OC4 semi-submersible considered in this work.

Table 1: Properties of the default mooring and IMS line segments in OrcaFlex

	Length $[m]$	Diameter $[m]$	Mass Density $[kg \cdot m^{-1}]$	Axial Stiffness $[MN \cdot m^{-1}]$
Default	832.8	0.08	113.4	753.6
IMS	2.7 - 4.0	0.30	70.7	0.1 - 7.6

The FOWT was simulated in both an operational and extreme load case, with the former at the rated speed of the wind turbine ($11.4\ m \cdot s^{-1}$) and the latter comparable to a 1:50 year storm event in the North Sea [25]. The turbine follows a conventional variable-speed, variable-pitch control strategy, as described in [26]. However, for the extreme case it was necessary to shut down the generator with the rotor blades feathered out of the wind using the recommended parked turbine aerodynamic modelling settings in [27]. Tower drag effects were included in the extreme load case because its influence was considered to be significant in high winds (50 $m \cdot s^{-1}$), but this was neglected for the operational case because the rotor thrust is the dominating drag force above the floating platform.

The unsteady wind files were created in TurbSim [28] using the von Karman spectral model, with the operational load case using the IEC normal turbulence model with turbulence characteristic A specified and the scaling from the 61400-1 standard [29]. Meanwhile the extreme wind model with a 50 year recurrence period was used for the extreme load case. In OrcaFlex, JONSWAP spectra were used to define the wave conditions, configured to travel in the same direction as the wind. The wind speed, v, significant wave height, H_s, peak period, T_p, and JONSWAP peak enhancement factor, γ, are summarized in Table 2 for each load case. Each simulation had a duration of 3 hours, which required the usage of periodic wind data files of duration 600 seconds each.

Table 2: Environmental conditions for each load case, duration: 3 hours

Load Case	v $[m \cdot s^{-1}]$	H_s $[m]$	T_p $[s]$	γ $[-]$
Operational	11.4	6	11	2.9
Extreme	50.0	11	17	1.0

3.3.2. Physical Implementation

Separate simulations were run in the model using the measured semi-static load-extension curves for each pre-charge case. The time-series results from the mooring line that experienced the greatest loading in the simulations were then exported in order to subject the device to the same conditions for the physical tests. All simulations were run twice on the test rig, once each in displacement and force mode using the extension and tension time-series results respectively. It was also necessary to Froude scale down the numerical results

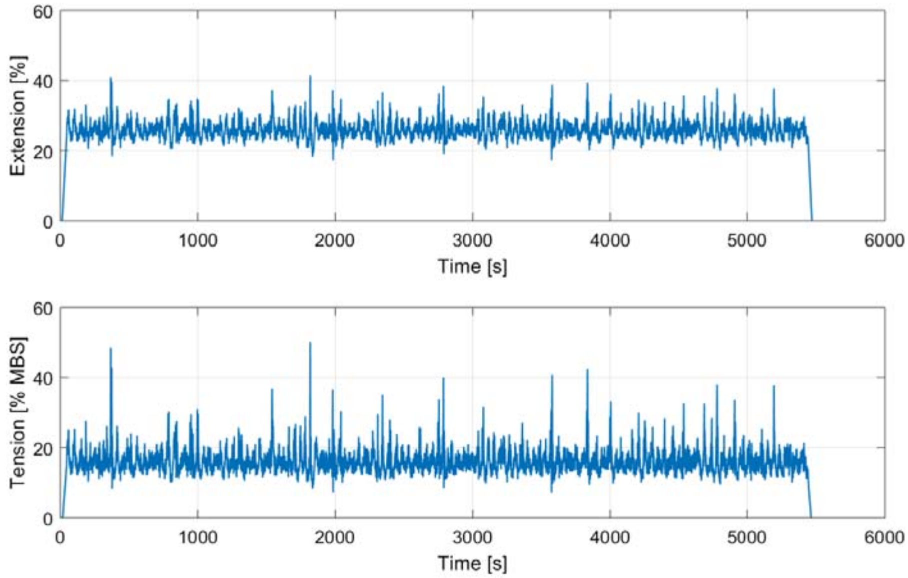

Figure 6: Extreme sea state time-series of extension (top) and tension (bottom) the IMS was subject to in displacement and force mode respectively

by a factor of 4 to ensure that the loads were suitable for the physical prototype. This meant that each physical simulation lasted 1.5 hours instead of 3. Due to time constraints, the physical simulations were not performed for the 310 kPa pre-charge case, although the predicted numerical results are presented later in Section 4.3.

Figure 6 shows the test profile for one of the extreme sea state load cases, derived after scaling down the numerical model results from the mooring line subject to the greatest loading. This mooring line only is studied in the analysis that follows and corresponds to the upwind line that runs parallel to the dominant wave and wind directions. The extension time-series was used to firstly subject the IMS prototype to these conditions on the test rig in displacement mode, while the tension time-series was subsequently run separately with the rig operating in force mode.

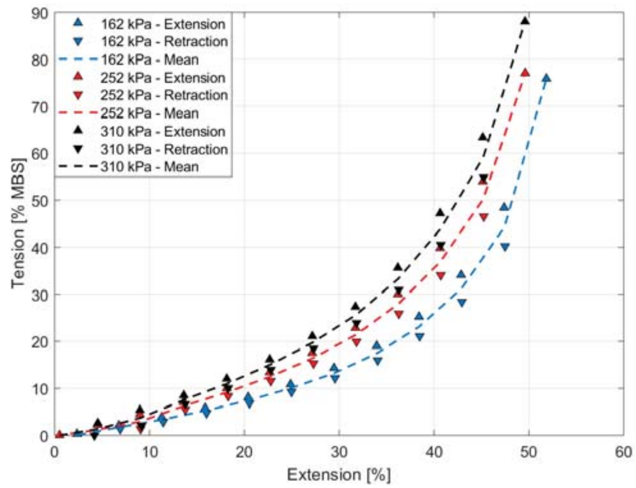

Figure 7: Semi-static load-extension behaviour of the IMS as a function of accumulator pre-charge pressure (blue, red, black)

4. Results

4.1. Semi-Static Tests

The results from the semi-static tests, as detailed in Section 3.1, are shown in Figure 7 for all 3 accumulator pre-charge configurations. The upwards arrows denote the mean values obtained within each stepping period during braid extension, while the downwards arrows denote the equivalent during retraction. The dashed lines are the mean of these values at each IMS point of extension. As mentioned previously in Section 3.3.1, these mean curves were used to represent the IMS in the numerical model.

For all of the results presented in Figure 7, it is clear that the IMS performance is characterised by a soft and elastic initial response, before developing considerable stiffness at larger extensions, i.e. the behaviour of the device is inherently non-linear. Consider, for example, the mean performance curve for the 162 kPa pre-charge condition. The tension in this case is less than 15% MBS at 30% extension, while this increases to over 75% MBS when the IMS is pulled to just over 50% extension.

It is also evident that the IMS load-extension behaviour is hysteretic, requiring greater tensions to elongate the device during the extension of the braid when compared with retraction. For example, the 310 kPa pre-charge condition required a tension of 63% MBS to pull the IMS to 45% extension, whereas during the retraction the required tension is 55% MBS.

The performance curves have a clear dependence on the initial accumulator configuration, with the developed braid stiffness being proportional to the pre-charge pressure. In addition to this, the performance of the device is dependent on the volume of the IMS bladder and its deformation with respect to extension. Any changes to this, for example a permanent deformation of the bladder, will affect how pressure in the device builds with extension, ultimately changing its load-extension curve. To determine if the device is susceptible to this type of change, the semi-static tests were repeated at various points throughout the test campaign to assess performance repeatability. These tests usually occurred at the beginning and end of each day. Figure 8 compares the measurements from two semi-static tests performed during the most intensive day of testing, where the IMS was subject to 6 hours of conditions representative of operating at sea (see Section 4.3). The results show a high degree of performance repeatability, with a mean absolute error (MAE) and a root mean square error (RMSE) of 0.4% and 0.6% found respectively. These findings were observed consistently throughout the test campaign for all configurations.

4.2. Dynamic Tests

To illustrate the difference between the semi-static and dynamic performance of the IMS, Figure 9 compares the 252 kPa test results from the 0.05 Hz cycling test with those presented previously in Figure 7. The dynamic results, which are from the final cycle in this test, form a larger hysteresis loop than in the semi-static case, with generally greater and lower tensions found during loading and unloading respectively. The peak tension at 45% extension is 60% MBS in the dynamic results, whereas it is 54% MBS in the semi-static case.

The size of the hysteresis loop formed is dependent on the cycling frequency,

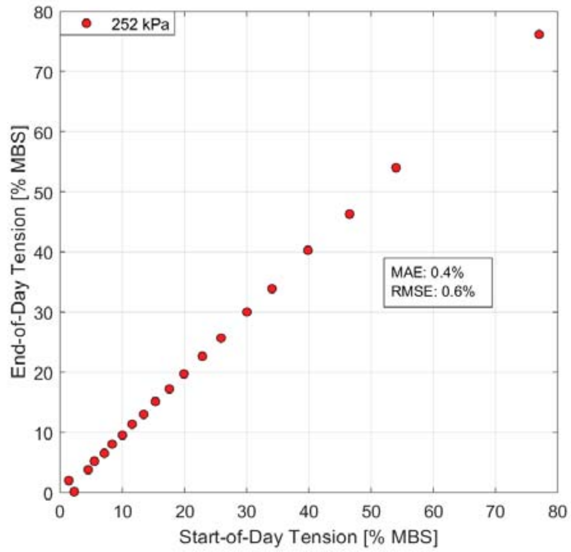

Figure 8: Semi-static load-extension measurements obtained at the start (x-axis) and end (y-axis) of a full test day

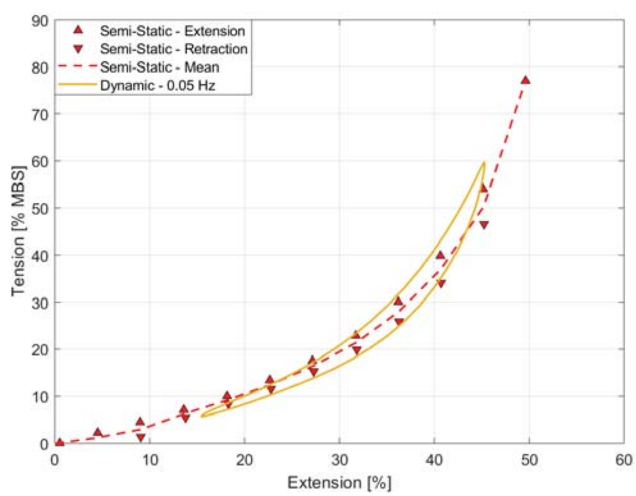

Figure 9: Comparison of semi-static (arrows and dashed line) and dynamic (solid line) load-extension behaviour for the 252 kPa case

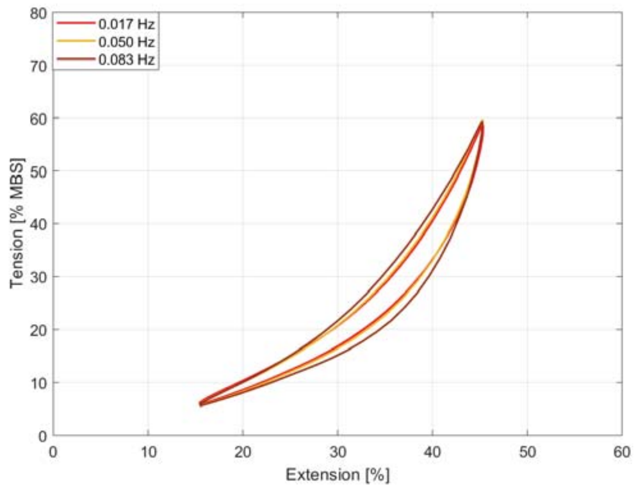

Figure 10: Hysteresis loops formed by cycling the IMS at 0.017 Hz (red), 0.050 Hz (yellow) and 0.083 Hz (brown) for the 252 kPa case

or load application rate, as shown in Figure 10 where the 252 kPa dynamic test results are shown for 3 selected frequencies. The tension increases during the loading part of the cycle with respect to frequency, while the opposite is true during unloading. Thus the loop size is proportional to the cycling frequency. However, peak and minimum tensions do not change significantly with cycling frequency. The results here also imply that the hysteresis loop size increases with load amplitude, provided that the frequency of the loading event is unchanged

The area bound by each hysteresis loop is a measure of the energy dissipated by the system. This can be quantified via numerical integration, where the total energy dissipated, E_d, is the difference between the areas under the load-extension curves formed during loading, E_{load}, and unloading, E_{unload}:

$$E_d = E_{load} - E_{unload} \tag{1}$$

Figure 11 shows the energy dissipated by the IMS as a function of cycling frequency and pre-charge pressure, calculated using a trapezoidal integration method. All of the results have been normalised by the energy dissipated by

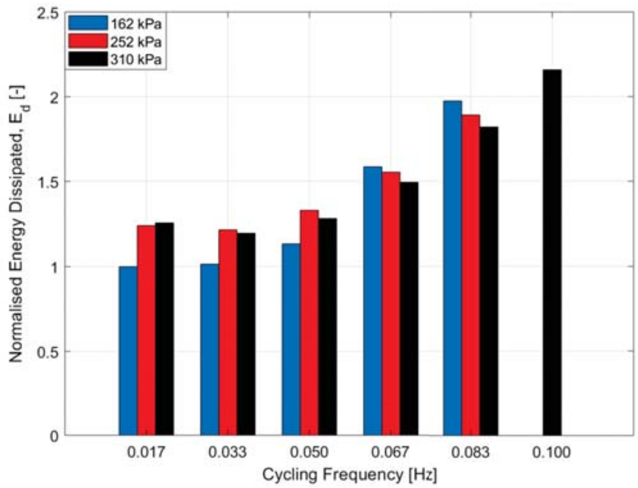

Figure 11: Energy dissipated by the IMS as a function of cycling frequency and pre-charge pressure, with all values normalised by the energy dissipated in the 162 kPa case at 0.017 Hz

the IMS at the lowest cycling frequency (0.017 Hz) and pre-charge pressure (162 kPa). Note that the IMS was only cycled at 0.100 Hz in the 310 kPa pre-charge case. These results further confirm that the energy dissipated by the IMS is proportional to the cycling frequency. While only modest increases in the dissipated energy are found between 0.017 - 0.050 Hz and in some cases a slight decrease is observed, at higher frequencies the difference is significant. For example, in the 162 kPa case the energy dissipated at 0.050 Hz is just 1.13, whereas this increases to 1.97 at 0.083 Hz. At the lowest frequency the energy dissipated increases with pre-charge pressure, but this is the only instance in which this result is found. The greatest amount of energy is dissipated by the 252 kPa configuration during the 0.033 and 0.050 Hz cycling, while at the highest frequencies the 162 kPa configuration dissipates the most. Thus, at higher frequencies the energy dissipated decreases with pre-charge pressure, contradicting the low frequency results.

This result is attributable to the differing internal pressure behaviour at low and high cycling frequencies, as shown in Figure 12. At low frequencies, there

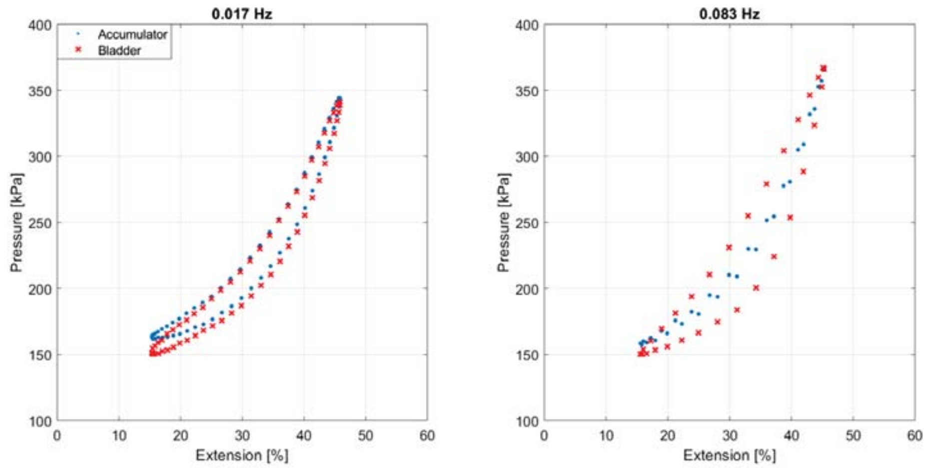

Figure 12: Accumulator (blue) and bladder (red) pressure hysteresis behaviour during low (left) and high (right) frequency cycling of the IMS with 162 kPa pre-charge

is an insignificant difference in the accumulator and bladder pressures as the braid is loaded and unloaded slowly. However, at high frequencies the bladder pressure increases and decreases at a greater rate during loading and unloading respectively compared with the accumulator, forming a larger hysteresis loop which leads to the increased energy dissipation observed previously (Figure 1). In contrast to this, the accumulator forms a smaller pressure hysteresis loop at higher frequencies. The differing accumulator and bladder hysteresis behaviour at high frequencies is due to limitations on the flow rate between these two systems. The higher bladder pressure observed during loading occurs because it cannot vent the fluid quick enough. A similar effect occurs during unloading, whereby pressure in the bladder is instead lost because the fluid has not returned quick enough from the accumulator. The hysteretic behaviour can be reduced to a degree by increasing the pre-charge pressure of the accumulator, which in turn increases the flow rate. This accounts for the trend of reduced energy dissipated with increasing pre-charge pressure found previously in Figure 1 at higher frequencies.

At the frequencies tested above 0.050 Hz for the 310 kPa pre-charge case

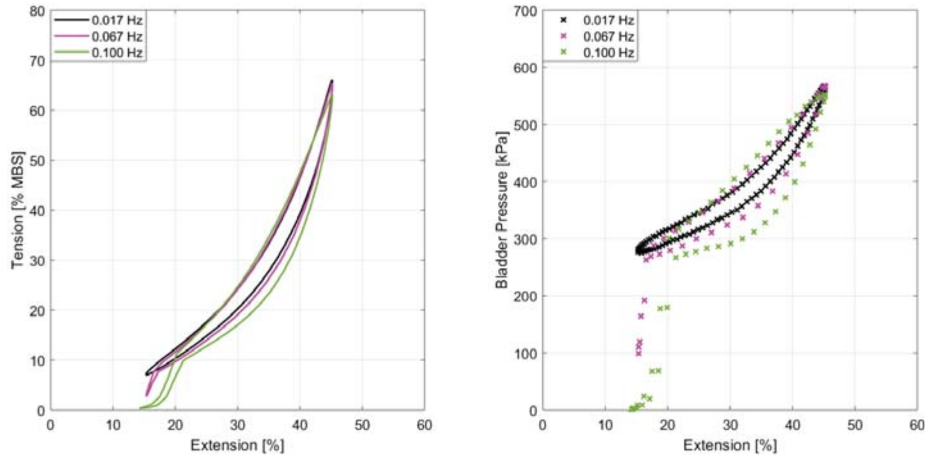

Figure 13: Load-extension (left) and internal bladder pressure (right) behaviour during the cycling of the IMS with 310 kPa pre-charge

only, a considerable reduction in tension is found to occur at low extensions during cycling, as shown in Figure 13. The reduction in tension becomes more significant with increasing cycling frequency, while the affected extension range also increases. This is caused by a loss of pressure at these extensions that only occurs during high frequency cycling. In addition to this, the peak loading is just 63.1% MBS during the 0.100 Hz cycling, compared with 66.0% and 65.5% MBS at 0.017 and 0.067 Hz respectively. This is the only notable reduction in peak loading that occurred during the dynamic tests, but the other pre-charge cases were not tested at this frequency.

4.3. Sea State Tests

The measured load-extension results from the physical simulations, as described in Section 3.3, are displayed on scatter plots in Figure 14, compared with the mean semi-static curves (as used in the numerical model) and 0.083 Hz hysteresis loops reported previously in Sections 4.1 and 4.2 respectively. The first observation is that there is a considerable difference between the displacement and force mode results. This should be expected given that a single load-extension curve was used to represent the IMS in OrcaFlex, while the dynamic

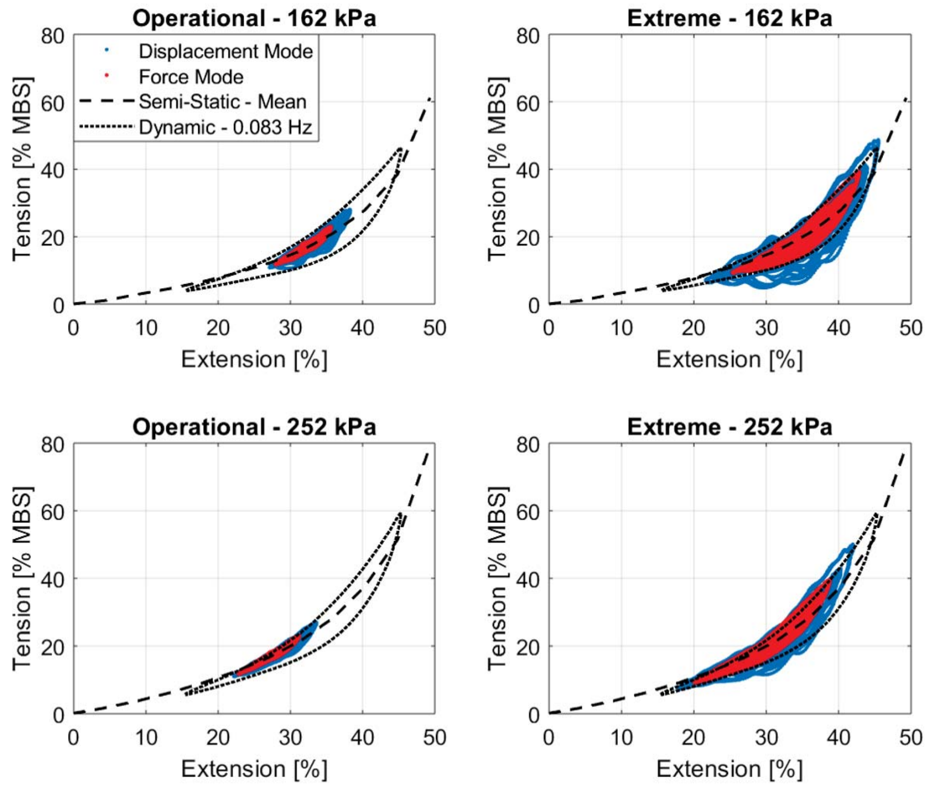

Figure 14: Load-extension behaviour of the IMS in displacement (blue) and force (red) mode during operational (left) and extreme (right) conditions for the 162 kPa (top) and 252 kPa (bottom) pre-charge cases, compared with previous semi-static (black dashed line) and dynamic (black dotted line) observations

behaviour of the physical device differs considerably to this (Section 4.2). The model assumes that the device is more compliant under loading than in reality, leading to the physical braid being extended further and developing greater tensions in displacement mode. Similarly, the model assumes that the braid must retract further to unload the device to some of the lowest loads, whereas dynamically these are found earlier at higher extensions. The overall effect is that there is a greater range in both extension and tension in the displacement mode results.

Generally, the scatter from operating in a sea state is all found to lie within the 0.083 Hz hysteresis loops, especially for the operational load case results. Some exceptions are found during the extreme load cases, particularly in the displacement mode results and in the 162 kPa pre-charge configuration. These occur during events in which the rate of change in displacement is greater than the 0.083 Hz cycling. This gives further evidence of the hysteretic behaviour of the IMS increasing with load application rate (Figure 10). In addition to this, there are a few instances in the 162 kPa extreme results in displacement mode where the tension is notably low despite the braid being at a moderate extension. For example, there are events in which the tension decreases to less than 5% MBS at 30% extension, whereas in the 252 kPa results the tension is always at least 11% MBS at this extension. This finding supports the reported inversely proportional relationship of energy dissipation and system pre-charge pressure under high frequency loading (Figure 11).

Figure 14 also shows that there is little difference between the mean and peak loads found between the two pre-charge cases. This is supported further through the results in Table 3, where the load reductions relative to the baseline OC4 mooring arrangement, i.e. without the inclusion of the IMS, are stated for both load cases and each IMS pre-charge. The 310 kPa simulation results are included for completeness, despite not being tested physically. This comparison, therefore, is effectively based on force mode results only. Each IMS configuration leads to a reduction in both the mean and peak mooring loads in all conditions, but its influence is most significant on the ultimate loads found in extreme conditions. In this load case, the peak loads are reduced by 8.6 - 9.4%. There is a trend of decreasing load reduction effectiveness with increasing pre-charge pressure, although it should be reemphasised that the differences are small.

Figure 15 compares the time-series of the measured IMS tension (force mode only) for the 162 kPa configuration with the baseline OC4 mooring tension over a 300 second period in the extreme sea state test. The greatest difference in these two sets of results is found during the significant loading event at 1780 seconds, where the baseline OC4 mooring tension is reduced from 44% to just under 40% with the inclusion of the IMS. This further highlights the effectiveness of the

Table 3: Mean and peak load reductions found with the inclusion of the IMS, relative to the baseline OC4 mooring arrangement

	Operational		Extreme	
	Mean	Peak	Mean	Peak
162 kPa	2.0%	2.8%	2.5%	9.4%
252 kPa	1.7%	2.3%	2.1%	8.9%
310 kPa	1.5%	2.0%	1.9%	8.6%

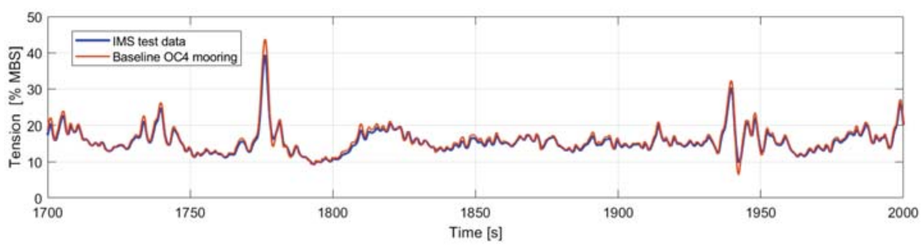

Figure 15: Time-series of measured IMS tension (blue) compared with the modelled baseline OC4 mooring tension (red) during the extreme sea state. The test data are from the 162 kPa configuration whilst operated in force mode

IMS in reducing peak loads. Elsewhere, moderate reductions in line tension are observed.

5. Discussion

The presented results demonstrate that the performance characteristics of the IMS are pressure dependent. This presents both opportunities and challenges for the application of the device. The ability to change the pressure of the device whilst deployed allows the in-operation tuning of the mooring system response, perhaps on a sea state basis. A simple strategy might be to stiffen the device response in storm conditions to limit platform motions, whereas in normal sea states the system pressure is reduced to minimise line loading. Prior work has also shown that a stiffer response can in some occasions reduce peak mooring line loads in extreme conditions as it limits platform accelerations in large waves [15, 23], although this was not found during such simulations for the configurations tested here. This behaviour will be critically dependent on the floating platform configuration and turbine control strategy. More accurate assessments will require close collaboration with technology developers, above and beyond the OC platform reference models.

The IMS response versatility is a key advantage over other mooring systems, but further work is required to better understand the dynamic features observed at both low and high pre-charge pressures. The variation in device performance was found to increase with cycling frequency (Figure 11). This contrasts some other highly non-linear mooring systems which show very little variation in performance with loading frequency [11]. The flow rate between the IMS accumulator and bladder has a crucial role in this, and a less restrictive flow control valve between these two components would reduce the dynamic behaviour. As part of ongoing work to support the development and design optimisation of the IMS, the device has been modelled as a hydraulic system to be able to predict these flow dependent dynamic characteristics [14].

Generally the hysteretic behaviour decreased with higher pre-charge pressures due to the fact that the flow rate improved in these cases. However, a complete bladder pressure loss was observed during the high frequency retraction of the IMS in the 310 kPa pre-charge case only (Figure 13). This is believed to be due to small, temporary deformations in the bladder shape after a period of loading. Any slight increase in bladder volume for a given extension will lead to a pressure decrease. The bladder pressure always recovered to the pre-charge level after leaving it for a period of rest, implying that the volume contracted back to its original shape. Similar pressure losses and subsequent recoveries were also observed in the lower pre-charge cases, but these occurred at extensions lower than the cycling range used in the dynamic tests (Section 3.2).

The load reduction potential of the IMS is difficult to quantify because the numerical model cannot capture the dynamic stiffness of the braid, with the mean semi-static performance curves used as an input. This also highlights one of the shortcomings of this type of physical testing, where the dynamic mooring forces and motions cannot be reproduced simultaneously [30]. In displacement mode, the braid is assumed to be much more elastic than in reality, leading to overestimated ranges of motion and tension. Similarly, the numerical model will underpredict peak tensions because under dynamic conditions the physical device is stiffer than modelled. However, the mean and peak loading results in Figure 14 are very similar between the pre-charge cases, despite the 252 kPa load-extension curve being stiffer. It can be argued, therefore, that the dynamic behaviour is insignificant for assessing load reduction in the cases considered. Hence each of the achieved load reductions stated in Table 3 will be slightly optimistic, but there is enough supplementary evidence to suggest that a reduction in peak loading in the region of 9% is achievable with the device tested. Previous work has shown that if the component can be built at a larger scale the load reduction potential increases [23], although this is accompanied by an increase in platform surge motions due to the added compliance in the mooring lines. These claims are supported by further extreme simulations which were run with longer IMS sections in the numerical model using the same mean dimensionless load-extension curves (Figure 7). The results are shown in Figure 16 from this analysis, suggesting that an IMS built with a 20 m braid length could reduce peak loads by more than 40%, or in excess of 25% at 10 m scale. This is an encouraging initial performance appraisal, but specific load reductions will have to be determined in close collaboration with technology developers as part of a systems engineering approach, ensuring that the influence of the mooring system on other aspects of the FOWT are considered.

6. Conclusions

The performance of a hydraulic mooring component, called the IMS, has been characterised during large-scale component tests, covering a range of conditions. Testing demonstrated the non-linear stiffness characteristics of the de-

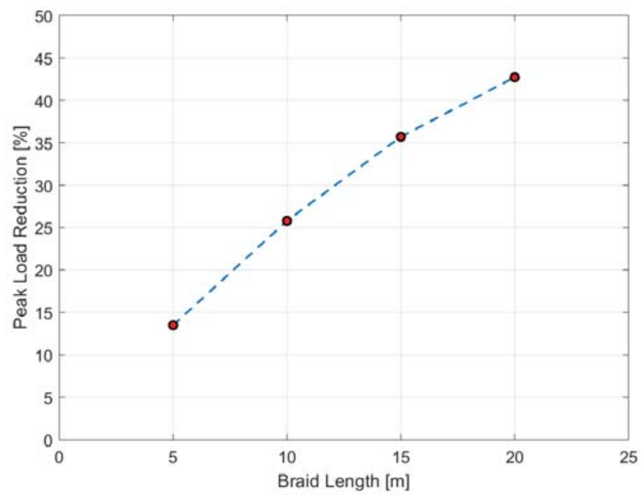

Figure 16: IMS peak load reduction potential as a function of braid length

vice, which can be varied by changing the system pre-charge pressure. This is a feature that distinguishes the IMS from other non-linear mooring systems. The performance of the device is inherently hysteretic in dynamic conditions, leading to a degree of performance variability dependent on load history and rate, as well as pre-charge pressure. Much of this behaviour arises from the continuous transfer of internal fluid between the accumulator and bladder, and can be determined via hydraulic modelling, which is the subject of ongoing work.

The IMS was also physically tested in conditions representative of an offshore deployment, after firstly deriving these from a numerical model. The device was modelled as part of the mooring system for the OC4 semi-submersible FOWT, using the FAST-OrcaFlex interface. The time-series results from the model simulations were then subsequently used to subject the IMS prototype to the same conditions in the test rig. The results suggest that the inclusion of the IMS would lower both mean and peak mooring line tensions, compared with the default mooring arrangement. A 9% reduction in peak loads was found in extreme conditions. While this represents a modest load reduction, the result is considered promising given the small scale of the prototype. Building the device at a scale in excess of 10 m will be key to realising the load reduction potential of the IMS for the FOWT application.

The presented work offers a methodology to de-risk innovative mooring systems, by determining the peak load reduction potential and physical performance through combining numerical modelling and large-scale physical testing. The results of such a test campaign support not only the certification of novel mooring systems, but will give floating offshore technology developers a benchmark regarding the potential opportunities and challenges of innovative mooring systems.

Acknowledgements

The research in this paper was undertaken as part of a collaborative project between Teqniqa Systems Ltd., the University of Exeter and DNV GL. The project received funding from Innovate UK, project reference: 103889. The authors wish to thank Orcina Ltd. for the provision of the OrcaFlex software, while they are also grateful to NREL for making the FOWT models freely available.

References

[1] WindEurope, Offshore Wind in Europe - Key trends and statistics 2018, Tech. rep., WindEurope (2019).

[2] Smith, A. and Stehly, T. and Musial, W., 20142015 Offshore Wind Technologies Market Report - NREL/TP-5000-64283, Tech. rep., National Renewable Energy Laboratory (NREL) (2015).

[3] The European Wind Energy Association (EWEA), Deep Water - The Next Step for Offshore Wind Energy, Tech. rep., EWEA (2013).

[4] B. Skaare, Development of the hywind concept, in: Proceedings of the ASME 2017 36th International Conference on Ocean, Offshore and Arctic Engineering (OMAE), Trondheim, Norway, 2017.

[5] D. Roddier, C. Cermelli, A. Aubault, A. Weinstein, Windfloat: A floating foundation for offshore wind turbines, Journal of Renewable and Sustainable Energy 2. doi:https://doi.org/10.1063/1.3435339.

[6] Equinor, World's first floating wind farm has started production, https://www.equinor.com/en/news/worlds-first-floating-wind-farm-started-production.html, accessed: 2019-08-05.

[7] The Carbon Trust, Floating Wind Joint Industry Project Phase I Summary Report, Tech. rep., The Carbon Trust (2018).

[8] The Carbon Trust, Floating Offshore Wind: Market and Technology Review, Tech. rep., The Carbon Trust (2015).

[9] S. Weller, L. Johanning, P. Davies, S. Banfield, Synthetic mooring ropes for marine renewable energy applications, Renewable Energy 83 (2015) 1268–1278. doi:https://doi.org/10.1016/j.renene.2015.03.058.

[10] T. Gordelier, D. Parish, P. Thies, S. Weller, P. Davies, P. L. Gac, L. Johanning, Assessing the performance durability of elastomeric moorings: Assembly investigations enhanced by sub-component tests, Ocean Engineering 155 (2018) 411–424. doi:https://doi.org/10.1016/j.oceaneng.2018.02.014.

[11] P. Thies, L. Johanning, P. McEvoy, A novel mooring tether for peak load mitigation: Initial performance and service simulation testing, International Journal of Marine Energy 7 (2014) 43–56. doi:http://dx.doi.org/10.1016/j.ijome.2014.06.001.

[12] T. Gordelier, D. Parish, P. Thies, S. Weller, L. Johanning, A novel mooring tether for highly-dynamic offshore applications; mitigating peak and fatigue loads via selectable axial stiffness, Journal of Marine Science and Engineering 3 (2015) 1287–1310. doi:https://doi.org/10.3390/jmse3041287.

[13] S. Weller, P. Davies, A. Vickers, L. Johanning, Synthetic rope responses in the context of load history: Operational performance, Ocean Engineering 83 (2014) 111–124. doi:https://doi.org/10.1016/j.oceaneng.2014.03.010.

[14] M. Harrold, P. Thies, D. Newsam, C. Bittencourt Ferreira, L. Johanning, Modeling a non-linear mooring system for floating offshore wind using a hydraulic cylinder analogy, in: Proceedings of the ASME 2019 38th International Conference on Ocean, Offshore and Arctic Engineering, Glasgow, UK, 2019.

[15] J. Luxmoore, S. Grey, D. Newsam, L. Johanning, Analytical performance assessment of a novel active mooring system for load reduction in marine energy converters, Ocean Engineering 124 (2016) 215–225. doi:https://doi.org/10.1016/j.oceaneng.2016.07.047.

[16] J. Luxmoore, P. Thies, S. Grey, D. Newsam, L. Johanning, Performance and reliability testing of an active mooring system for peak load reduction, Proceedings of the Institution of Mechanical Engineers, Part M: Journal of Engineering for the Maritime Environment 232 (2018) 130–140. doi:https://doi.org/10.1177/1475090217716859.

[17] P. Thies, L. Johanning, K. Karikari-Boateng, C. Ng, P. McKeever, Component reliability test approaches for marine renewable energy, Proceedings of the Institution of Mechanical Engineers, Part O: Journal of Risk and Reliability 229 (2015) 403–416. doi:https://doi.org/10.1177/1748006X15580837.

[18] International Organization for Standardization (ISO), ISO/TS 19336. Fibre ropes for offshore station keeping Polyarylate, Tech. rep., International Organization for Standardization (ISO) (2015).

[19] M. Masciola, A. Robertson, J. Jonkman, F. Driscoll, Investigation of a fast-orcaflex coupling module for integrating turbine and mooring dynamics of offshore floating wind turbines, in: Proceedings of the International

Conference on Offshore Wind Energy and Ocean Energy, Beijing, China, 2011.

[20] Jonkman, J. and Buhl, M., FAST User's Guide - NREL/EL-500-38230, Tech. rep., National Renewable Energy Laboratory (NREL) (2005).

[21] Orcina, Orcaflex documentation, `https://www.orcina.com/resources/documentation/`, accessed: 2019-07-26.

[22] Robertson, A. and Jonkman, J. and Masciola, M. and Song, H. and Goupee, A. and Couling, A., and Luan, C., Definition of the Semisubmersible Floating System for Phase II of OC4 - NREL/TP-5000-60601, Tech. rep., National Renewable Energy Laboratory (NREL) (2014).

[23] M. Harrold, P. Thies, L. Johanning, D. Newsam, M. Checkley, C. Bittencourt Ferreira, Dynamic load reduction and station keeping mooring system for floating offshore wind, in: Proceedings of the International Offshore Wind Technical Conference (IOWTC), San Francisco, USA, 2018.

[24] Jonkman, J., Definition of the Floating System for Phase IV of OC3 - NREL/TP-500-47535, Tech. rep., National Renewable Energy Laboratory (NREL) (2010).

[25] Williams, M., Wave Mapping in UK Waters - RR392, Tech. rep., HSE Books (2005).

[26] Jonkman, J., and Butterfield, S., and Musial, W., and Scott, G., Definition of a 5-MW Reference Wind Turbine for Offshore System Development - NREL/TP-500-38060, Tech. rep., National Renewable Energy Laboratory (NREL) (2009).

[27] Jonkman, J. and Hayman, G. and Jonkman, B. and Damiani, R., AeroDyn v15 Users Guide and Theory Manual - Draft Version, Tech. rep., National Renewable Energy Laboratory (NREL) (2017).

[28] Jonkman, B. and Kilcher, L., TurbSim Users Guide: Version 1.06.00 Draft Version, Tech. rep., National Renewable Energy Laboratory (NREL) (2012).

[29] International Electrotechnical Commission (IEC), IEC 61400-1: Wind Turbines Part 1: Design Requirements Third Edition, Tech. rep., IEC (2005).

[30] M. Harrold, P. Thies, P. Halswell, L. Johanning, D. Newsam, C. Bittencourt Ferreira, Demonstration of the intelligent mooring system for floating offshore wind turbines, in: Proceedings of the International Offshore Wind Technical Conference (IOWTC), St. Julian's, Malta, 2019.